Q. J. R. Meteorol. Soc. (2005), **131**, pp. 565–579 doi: 10.1256/qj.04.47

How homogeneous and isotropic is stratospheric mixing? Comparison of CRISTA-1 observations with transport studies based on the Chemical Lagrangian Model of the Stratosphere (CLaMS)

By P. KONOPKA[1]*, R. SPANG[1], G. GÜNTHER[1], R. MÜLLER[1], D. S. McKENNA[2], D. OFFERMANN[3] and M. RIESE[1]

[1]*Forschungszentrum Jülich, ICG-I, Jülich, Germany*

[2]*National Center for Atmospheric Research, Boulder, USA*

[3]*Department of Physics, University of Wuppertal, Germany*

(Received 18 March 2004; revised 6 October 2004)

SUMMARY

The Chemical Lagrangian Model of the Stratosphere (CLaMS) is used for the interpretation of N_2O observed during the CRISTA-1 experiment in early November 1994. By comparing CRISTA data with CLaMS simulations, the impact of the large-scale horizontal deformations on mixing is studied. Using the probability density function technique (PDF) quantifying the statistics of N_2O variability, the critical deformation γ_c was inferred that triggers the mixing algorithm in CLaMS. The critical deformation γ_c measures the ratio between the major and minor axes of the ellipse resulting from the stretching of a circle surrounding a given Lagrangian air parcel, i.e. only deformations stronger than γ_c are relevant for mixing in CLaMS.

The PDF derived from CRISTA observations at 700 K and on horizontal scales of the order of 200 km is characterized by a Gaussian core and non-Gaussian tails indicating filamentary structures typical for 2D turbulence. The PDFs obtained from CLaMS simulations strongly depend on γ_c but only weakly on the horizontal resolution r_0 that was varied between 45 and 200 km. The choice $\gamma_c = 0.8$ in the model best reproduces the observed PDF. This implies that the large-scale isentropic transport leads to scale collapse and subsequent mixing in those parts of the flow where on a time scale $\approx$12 hours and a spatial scale $\approx$200 km the flow stretches a circle to an ellipse with the ratio between the major and minor axes exceeding 5. Owing to the spatial resolution of the CRISTA instrument that smooths out the non-Gaussian tails, the elongation rate $\approx$5 estimates only the lower bound of the critical deformation.

Furthermore, our simulations show that air masses of low N_2O amounts observed by CRISTA between 20° and 40°S are fragments of the polar vortex that have been peeled from the vortex edge. The history of these fragments can be divided into two phases: formation and mixing of filaments at the vortex edge where $\gamma > \gamma_c$ and pure advection of the remnants of such filaments into midlatitudes in flow regions with $\gamma < \gamma_c$. Here, the lifetime of such remnants may exceed two weeks due to negligible mixing in these parts of the flow.

KEYWORDS: Chaotic advection Filamentation Polar vortex Turbulent diffusion

1. INTRODUCTION

Usually, mixing in fluid dynamics denotes the irreversible part of (tracer) transport. Inaccurate representation of mixing in photochemical transport models may influence the predictions of chemically active species (Edouard *et al.* 1996; Searle *et al.* 1998). Whereas the process of physical mixing occurs in the stratosphere on vertical scales of around 100 m and horizontal scales of the order of 10 km (Balluch and Haynes 1997) or possibly on even smaller scales (Tuck *et al.* 2003), photochemical transport models that are routinely used significantly overestimate mixing due to much coarser vertical and horizontal resolution of the order of 1 km and 100 km, respectively.

In the surf zone, the large-scale zonally symmetric flow is disturbed by planetary and synoptic-scale waves (McIntyre and Palmer 1983) giving rise to chaotic advection and two-dimensional (2D) turbulence (Ngan and Shepherd 1999a,b) that dissipate their kinetic energy by the horizontal scale collapse (Juckes and McIntyre 1987). A key feature of the chaotic advection in the stratosphere is that stretching on small scales is triggered by the large-scale winds, i.e. advection occurs within the so-called Batchelor regime (Haynes and Vanneste 2004). This property of transport explains the

* Corresponding author: Forschungszentrum Jülich, ICG-I, D-52425 Jülich, Germany.
e-mail: p.konopka@fz-juelich.de

success of the 'reverse domain filling' technique (RDF) (Sutton *et al.* 1994) and the 'contour advection with surgery' technique (CAS) (Norton 1994; Waugh and Plumb 1994) in reconstructing tracer structures that are not resolved by conventional meteorological analyses or coarse-resolution models (see e.g. Orsolini *et al.* 1997). The main shortcomings of these methods is the lack of controlled mixing between the air parcels (APs) and, until recently, only a 2D formulation of these techniques.

Stretching of air masses may increase the spatial gradients of trace substances and thereby reduce time-scales for mixing (Pierrehumbert 1991). Thus, one expects that sufficiently strong flow deformations and the associated high stretching or elongation rates will trigger stratospheric mixing. To some extent, the 'surgery' of the CAS technique can be considered as such a dissipative process (Dritschel 1989), however its coupling to the stretching rates is difficult to quantify.

The Chemical Lagrangian Model of the Stratosphere (CLaMS) is the first Chemistry Transport Model (CTM) based on Lagrangian transport where the concept of deformation-induced mixing was successfully realized both in two and three dimensions (McKenna *et al.* 2002; Konopka *et al.* 2004). The choice and validation of the mixing parameters for 2D and 3D versions of CLaMS is discussed in Konopka *et al.* (2003) and Konopka *et al.* (2004), respectively, where the agreement between the tracer distributions observed *in situ* and those simulated was optimized. This kind of comparison, both in the form of time series and tracer–tracer correlations, does not allow the underlying mixing parameters to be unambiguously derived. This is because the simulated tracer distribution is the result of an integral procedure, i.e. different mixing procedures may lead to the same tracer distribution. Thus, additional methods are necessary to determine the value of mixing parameters more precisely.

In this paper, we demonstrate how the probability density function (PDF) technique can be used (see e.g. Sparling 2000) to quantify the mixing parameters from N_2O distributions observed during the CRISTA-1 experiment in early November 1994. Recently, this technique was successfully used to describe simulated tracer fluctuations resulting from chaotic advection during isentropic tracer transport (Hu and Pierrehumbert 2001) and to derive the stratospheric dissipation scales from high-resolution aircraft measurements of ozone (Sparling and Bacmeister 2001). Although the spatial resolution of aircraft data is typically very high, their coverage is limited by the aircraft range. Thus, only a small part of streamers or filaments can be observed, usually in the form of time series along the aircraft track. In early November 1994, the Cryogenic Infrared Spectrometers and Telescopes for the Atmosphere (CRISTA) project measured thermal emissions (4–71 μm) of selected trace gases by limb scanning with high spatial resolution (Offermann *et al.* 1999). Structures of atmospheric tracer species were resolved with a resolution of 200 km in the horizontal and 2–3 km in the vertical.

The paper is organized as follows. In the next two sections, we briefly summarize the definition of the mixing parameters used in CLaMS and apply the concept of diffusion coefficients to discuss the inhomogeneity and anisotropy of CLaMS mixing. CRISTA observations and CLaMS initialization are presented in section 4. In section 5, by comparing the PDFs derived from the CRISTA observations and CLaMS simulations with different mixing scenarios, we show how the mixing parameters can be optimized. Finally, section 6 discusses our results and the conclusions are presented in section 7.

2. Mixing parameters in CLaMS

After initialization of the model, each of the transport steps consists of two parts—pure advection in terms of the trajectories, and subsequent mixing. The length of the

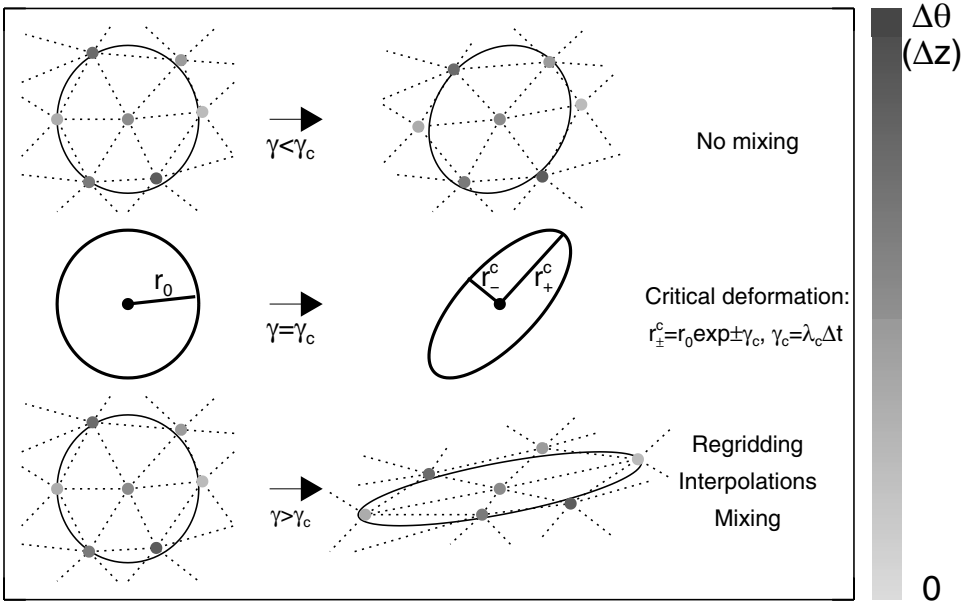

Figure 1. Deformation-induced mixing in CLaMS (for details see text and also McKenna *et al.* 2002, Konopka *et al.* 2004).

advection step Δt is constant for each transport step with typical values varying between 6 and 24 hours. Mixing in the model results from the adaptive regridding (with the frequency $1/\Delta t$) and associated interpolations on the new APs.

This procedure is shown schematically in Fig. 1, where a part of the horizontal irregular grid of APs is depicted with a mean horizontal separation r_0. In the 2D (isentropic) formulation, all APs have the same potential temperature θ (i.e. the same gray shading), and in 3D the APs are uniformly distributed in a horizontal layer with a thickness $\Delta\theta$ (or geometric thickness Δz) and with a mean vertical separation given by $\Delta z/2$. Thus, the aspect ratio α describing the ratio between the resolved horizontal and vertical scales is given by $2r_0/\Delta z$. During the advection step Δt, parts of the grid undergo deformation caused by horizontal strain (in the 2D case) or coupled horizontal strain and vertical shear (in 3D). In an incompressible flow, this deformation can be quantified by only one parameter γ measuring the major (r_+) and minor (r_-) axes of an ellipse, given by $r_\pm = r_0 \exp(\pm\gamma)$, and resulting from a deformation of a circle with the radius r_0 that surrounds a given AP. (2D incompressibility means $r_0^2 = r_+ r_-$, i.e. the circle and the ellipse have the same area). Thus, γ measures the eccentricity of the ellipse through $r_+/r_- = \exp(2\gamma)$.

If γ exceeds a prescribed value γ_c and, consequently, the conditions $r_+ > r_+^c = r_0 \exp(\gamma_c)$ and $r_- < r_-^c = r_0 \exp(-\gamma_c)$ are valid, the grid adaptation procedure 'reorders' the grid by insertion or merging of APs. Interpolation is necessary to determine the mixing ratios of tracer species on the new grid points. The associated numerical diffusion parametrizes mixing in the model. While the purely advective transport is completely reversible, this regridding procedure, which is driven by sufficiently strong flow deformations, defines the amount of irreversibility (i.e. mixing) affecting the transport of the chemical constituents.

The parameters γ (γ_c) can also be expressed in terms of the Lyapunov exponent λ (λ_c) using the relation $\gamma = \lambda \Delta t$ ($\gamma_c = \lambda_c \Delta t$) (McKenna *et al.* 2002; Konopka *et al.* 2004). In contrast to the parameter γ, the Lyapunov exponent λ does not depend on time for infinitesimally small time steps Δt. As we show in this paper, the currently available datasets allow γ_c to be inferred rather than λ_c and Δt. This is the reason why we decided to use the critical deformation γ_c here instead of the critical Lyapunov exponent λ_c to discuss the question of the inhomogeneity and anisotropy of stratospheric mixing.

In addition, the horizontal and vertical mixing processes between the APs depend on the mean horizontal and vertical separations that represent the approximate horizontal and vertical scales L_h and L_v resolved by the model. Haynes and Anglade (1997) argued that the average stratospheric value for the aspect ratio $\alpha = L_h/L_v$ is $\approx$250 and that α also estimates the ratio between the horizontal and vertical diffusivities D_h and D_v through $\alpha^2 = D_h/D_v$. Thus, the horizontal separation r_0 between the APs and the aspect ratio α together with the critical deformation γ_c and the regridding frequency $1/\Delta t$ are the parameters governing mixing in the 3D formulation of CLaMS.

The most important new feature of mixing in CLaMS is its spatial and temporal inhomogeneity as well as its anisotropy relative to the wind direction. These properties are controlled by the critical deformation γ_c (see Fig. 1), or the critical eccentricity $r_+^c/r_-^c = \exp(2\gamma_c)$. That is, deformations with $\gamma > \gamma_c$ trigger the regridding procedure and, consequently, cause mixing. Using satellite and *in situ* observations, we have shown in previous 2D studies that the best choice of γ_c is around 1 (McKenna *et al.* 2002; Konopka *et al.* 2003b). In the 3D studies, the choice $\gamma_c = 1.5$ leads to an optimal agreement between tracer distributions observed *in situ* and those simulated (Konopka *et al.* 2004).

3. Inhomogeneity and anisotropy of mixing

As described in the previous section (see Fig. 1), mixing in CLaMS can be understood as a consequence of the numerical diffusion due to adaptive regridding (insertion and merging of APs) and the associated interpolation of the mixing ratios on the new grid positions. In the 2D formulation of CLaMS, the horizontal diffusivity D_h associated with a singular interpolation is anisotropic with respect to the local (horizontal) wind and decomposes into D_+ (insertion) and D_- (merging), corresponding to mixing along and across the wind, respectively. The values of $D_\pm$ can be estimated as:

$$D_\pm(\gamma) = \begin{cases} D_{\text{eff}}^0 \exp(\pm 2\gamma) & \gamma \geqslant \gamma_c \\ 0 & \gamma < \gamma_c \end{cases}, \quad \text{with } D_{\text{eff}}^0 = \frac{r_0^2}{4\Delta t}, \tag{1}$$

where, in contrast to the formulation discussed in McKenna *et al.* (2002), λ, λ_c were replaced by γ, γ_c. According to (1), mixing is strongly inhomogeneous and occurs only in those parts of the grid that experienced sufficiently high deformation rates with $\gamma > \gamma_c$. The value of $D_\pm$ can be expressed as a product of two terms: D_{eff}^0 and $\exp \pm(2\gamma)$ describing its isotropic and anisotropic parts, respectively.

Assuming that Δz describes the thickness of the isentropic layer represented in CLaMS-2D, D_{eff}^0 can be rewritten as

$$D_{\text{eff}}^0 = \alpha^2 D_v \quad \text{with} \quad \alpha = \frac{2r_0}{\Delta z}, \quad D_v = \frac{(\Delta z)^2}{16\Delta t}. \tag{2}$$

Thus, in the 2D approach, the effective diffusivity D_{eff}^0 describes vertical mixing processes in the isentropic layer with the thickness $\Delta\theta$ and can be estimated from

the aspect ratio α and vertical diffusivity D_v (Balluch and Haynes 1997). For $\alpha \approx 250$ (Haynes and Anglade 1997) and D_v in the range 10^{-4} to 10^{-1} m^2s^{-1} (Waugh *et al.* 1997; Tan *et al.* 1998), D_{eff} is in the range 6×10^0 to 1.25×10^4 m^2s^{-1}. Thus, for CLaMS 2D studies, the choice of the parameters r_0 and Δt is limited by the requirement that the effective diffusivity is within this range.

In the 3D formulation, α (or Δz or the vertical diffusivity D_v) is an additional free parameter of the model that has to be optimized. Based on *in situ* data measured within the Arctic vortex in 1999/2000, Konopka *et al.* (2004) have shown that, in agreement with the results of Haynes and Anglade (1997), $\alpha = 250 \pm 100$ leads to the best description of the transport in the lower stratosphere. Thus, according to (2), the parameters r_0, α and Δt determine the vertical diffusivity D_v and the isotropic part of the horizontal diffusivity D^0_{eff}.

Relation (2) shows that, owing to the quadratic dependence on r_0 and Δz, the strongest impact on D^0_{eff} and D_v can be achieved by varying the spatial resolution of the model. The main limitation on Δt is the requirement that the neighbourhood relations between each AP and its nearest neighbours should not significantly change during the time step Δt, or, in other words, the deformation of a circle with radius r_0 can be approximated by an ellipse. Sensitivity studies with winds from the European Centre for Medium-Range Weather Forecasts and the UK Met Office (UKMO) show that Δt should be less than 24 hours in order to fulfil this requirement. The lower limit of Δt, i.e. $\Delta t = 6$ hours, is determined by the highest grid adaptation frequency that was used in this study.

The anisotropy of mixing, i.e. a strong difference between D_+ and D_-, is described in (1) by the function $f_\pm = \exp(\pm 2\gamma)$. In Fig. 2, $f_\pm$ is shown together with the eccentricity of the deformation ellipse r_+/r_-. For example, the choice $\gamma_c \approx 0.1$ means that the mixing is even triggered by very small deformations in the flow and, consequently, mixing can be expected everywhere (homogeneity). Furthermore, the difference between D_+ and D_-, i.e. the anisotropy, is negligible. The opposite situation can be expected for $\gamma_c \approx 1.0$. Here, mixing is switched on only if the flow stretches a circle with radius r_0 to an ellipse with $r_+/r_- > \exp(2\gamma_c) \approx 7$ and, owing to $D_+/D_- = \exp(4\gamma)$, D_+ (along the wind) exceeds D_- (across the wind) by a factor larger than 60 for $\gamma = \gamma_c = 1$.

Generally, the main limiting factor for modelling of the stratospheric transport and chemistry with the grid-based numerical models currently employed is their spatial resolution that exceeds, presumably by several orders of magnitude (Tuck *et al.* 2003), the expected dissipation scales. In contrast to the Eulerian approach, where the numerical diffusion is present always and everywhere due to interpolations of the transported field on the spatially fixed (Eulerian) grid, numerical diffusion in the Lagrangian formulation (CLaMS) occurs inhomogeneously (in time and space), i.e. it is triggered only by sufficiently strong deformations in the flow. According to Fick's law, $j = D\nabla\chi$, a strong diffusive flux j can be expected in regions with high diffusivity D and steep tracer gradient $\nabla\chi$. Contrary, strong tracer gradients can be preserved in regions with small diffusivity D (small deformations in the flow), e.g. across such transport barriers as the vortex edge (see Fig. 4 in McKenna *et al.* (2002)).

Furthermore, the Courant criterion requiring that an advected air parcel does not pass an Eulerian grid box of size r_0 during one time step Δt leads to a strong limitation of Δt of the order of 10 minutes for $r_0 \approx 200$ km (see e.g. Prather 1986), that is by a factor $\approx$70 smaller than the typical CLaMS time step $\Delta t = 12$ hours. Using relation (2), the Eulerian numerical diffusivity exceeds the Lagrangian diffusivity by the same factor. Thus, if compared with the Eulerian view, numerical diffusion in CLaMS may describe

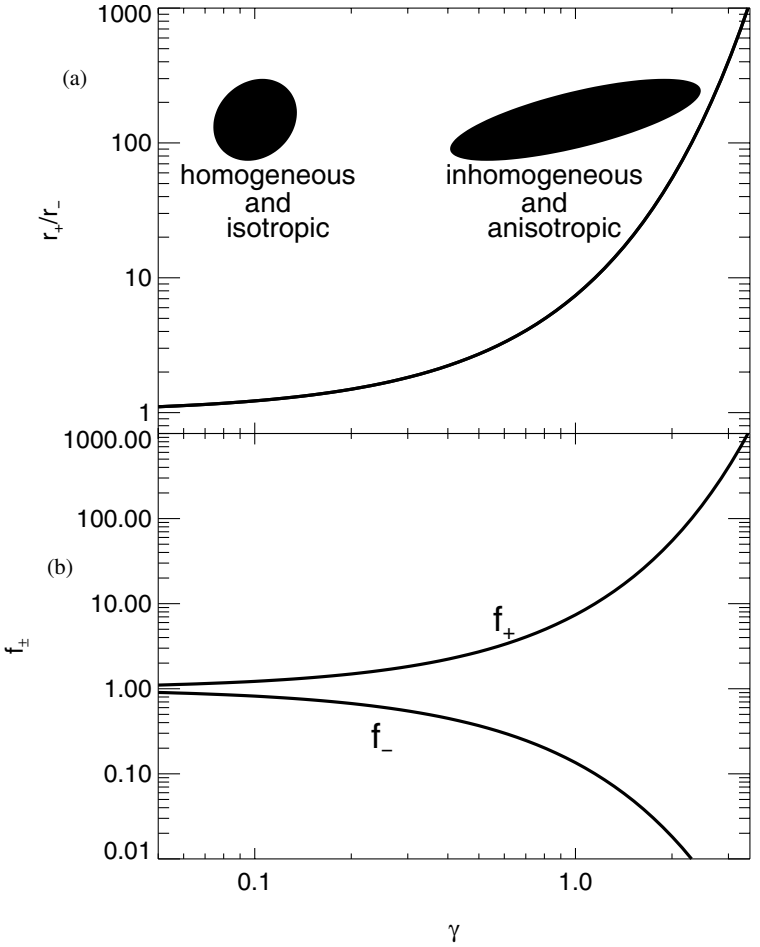

Figure 2. (a) Eccentricity of the deformation ellipse $r_+/r_- = \exp 2\gamma$ and (b) anisotropy of mixing $f_\pm = \exp \pm (2\gamma)$, both as a function of γ. CLaMS simulations suggest γ_c to be of the order $\approx$1, i.e. a strongly inhomogeneous and anisotropic mixing.

the atmospheric mixing more realistically because it is driven by the flow deformations (that are generally expected to drive the turbulence in the atmosphere) and because its absolute value can be significantly reduced.

4. CRISTA OBSERVATIONS OF N_2O IN NOVEMBER 1994 AND CLAMS SIMULATIONS

CRISTA-1 was launched on 3 November 1994 aboard the space shuttle *Atlantis* into a 300 km, 57° inclined orbit and between 4 and 12 November 1994 collected about 50 000 height profiles of limb radiance spectra with a latitudinal coverage from 57°S to 67°N. CRISTA measurements of N_2O at $\theta = 700$ K valid for 4 November are shown in Fig. 3(a).

Here, asynoptic profiles observed between 4 and 6 November 1994 were linearly interpolated in the vertical to $\theta = 700$ K and then transformed to the synoptic time of 12 UTC on 4 November, by the use of isentropic backward trajectories derived from UKMO winds. The sharp gradients of N_2O at the southern vortex edge and two areas A and B of low N_2O mixing ratios between 20°S and 40°S are evident in Fig. 3(a)

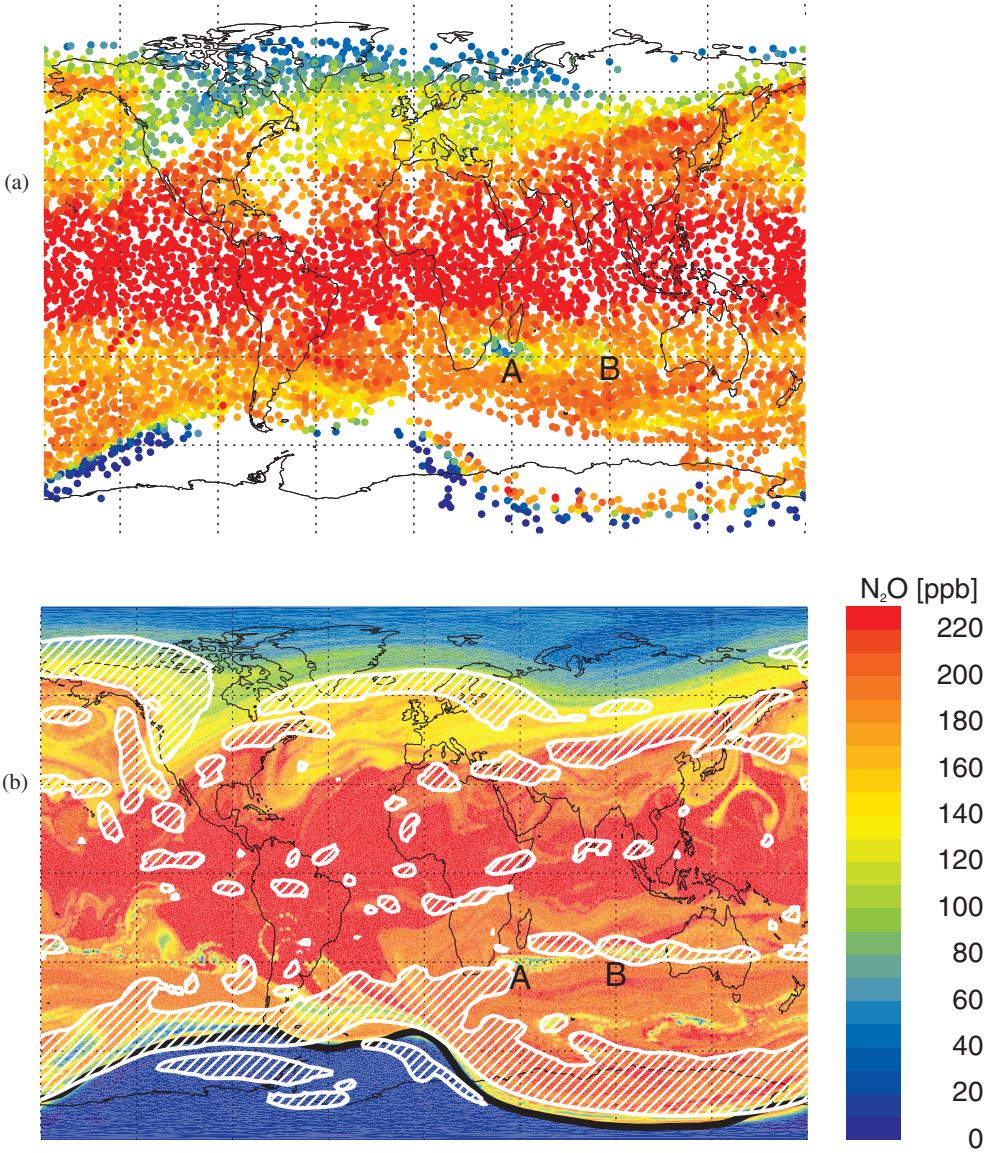

Figure 3. CRISTA observations of N_2O mixing ratios at $\theta = 700$ K versus CLaMS simulations: (a) Synoptic map on 4 November 1994, derived from CRISTA observations between 4 and 6 November 1994. (b) CLaMS distribution on 4 November 1994 resulting from isentropic transport with $\gamma_c = 0.8$. The white hatched contours denote mixing regions where during the last 12-hour advection step the condition $\gamma > \gamma_c$ was valid. The black line denotes the vortex edge derived from the Nash criterion. Two areas A and B of low N_2O between 20 and 40°S are fragments of polar vortex that have been peeled from the vortex edge and can also be seen in the corresponding CRISTA data.

and were discussed by Riese *et al.* (1999) and McKenna *et al.* (2002). Strong but less well-defined gradients are also observed across the streamers in the vicinity of the incipient northern vortex (Kouker *et al.* 1999; Riese *et al.* 1999). These phenomena were consistently observed between 4 and 10 November.

To initialize CLaMS, we apply the potential vorticity (PV)–N_2O correlation discussed by McKenna *et al.* 2002. We initialize CLaMS on 20 October, i.e. about two weeks before the first CRISTA observations are available. On the one hand, this period is long enough to study the influence of CLaMS mixing on the N_2O distributions and, on the other hand, the 2D (isentropic) version of CLaMS can be applied owing to negligible cross-isentropic transport on a time scale of three weeks. (Full 3D simulations, not shown, did not display significant differences, and the numerical costs are too high if the spatial resolution is higher than 80 km).

We expect that CLaMS should reproduce tracer variability similar to CRISTA (i.e. filaments and vortex remnants) if the model resolution is of the same order as the resolution of the measurement ($\approx$200 km). Thus, as a reference case, we employ a globally and initially uniform distribution of APs at the 700 K isentropic surface with the distance between the neighbouring APs $r_0 = 200$ km. To study the influence of the horizontal resolution on the tracer transport, we additionally consider initial distributions with a greater spatial resolution poleward of 10 °S with $r_0 = 100$, 65 and 45 km.

5. Probability distribution functions of the observed and simulated N_2O distributions

The study of the PDFs of tracer differences between APs separated by a prescribed distance offers an effective way to analyze the variability of tracer distributions (see e.g. Sparling 2000). In turbulent flows, an anomalously high probability of extreme spatial concentration fluctuations, termed 'intermittency', is expected and, consequently, the corresponding PDFs are characterized by a Gaussian core and non-Gaussian tails (see e.g. Shraiman and Siggia 2000).

In the following, PDFs of N_2O differences between APs at the 700 K isentropic surface are considered, both for the CRISTA synoptic observations between 4 and 11 November and the corresponding CLaMS simulations. For the reference case ($r_0 =$ 200 km), PDFs of N_2O differences are calculated for all pairs of APs separated by distances between 100 and 300 km and, due to the coverage of the CRISTA observations, with latitudes between 60°S and 70°N. By numbering the n APs from north to south, only pairs with $i < j$, $(i, j = 1, \ldots, n)$ are considered to avoid double counting (thus, the PDFs are not necessarily symmetric).

Figure 4 shows the PDF of all N_2O differences observed between 4 and 11 November (about 60 000 pairs). The observed PDFs have a Gaussian core ($\sim\exp\{-a(\Delta N_2O)^2\}$, $a = 0.0015$) that is most likely due to instrumental precision, and non-Gaussian tails (so-called 'fat tails') indicating an anomalously high probability of events with steep tracer gradients. These tails can be best fitted by the exponential function ($\sim\exp\{-a|\Delta N_2O|^p\}$, $a = 0.4$, $p = 0.63$, but other choices of p in the range $0.5 < p < 0.7$ also produce reasonable fits).

In Fig. 5 we compare the CRISTA observations with the PDFs calculated from the CLaMS simulations with different values of γ_c varying between ∞ (pure advection), and 0.4. The shape of the CLaMS PDFs shows a strong dependence on the value of γ_c. The fat tails of these PDFs are most pronounced in the pure advection run ($\gamma_c = \infty$ in Fig. 5(c)) and are increasingly smoothed out with a decreasing value of γ_c. The best representation of the CRISTA observations is independent of Δt and given by $\gamma_c \approx 0.8$.

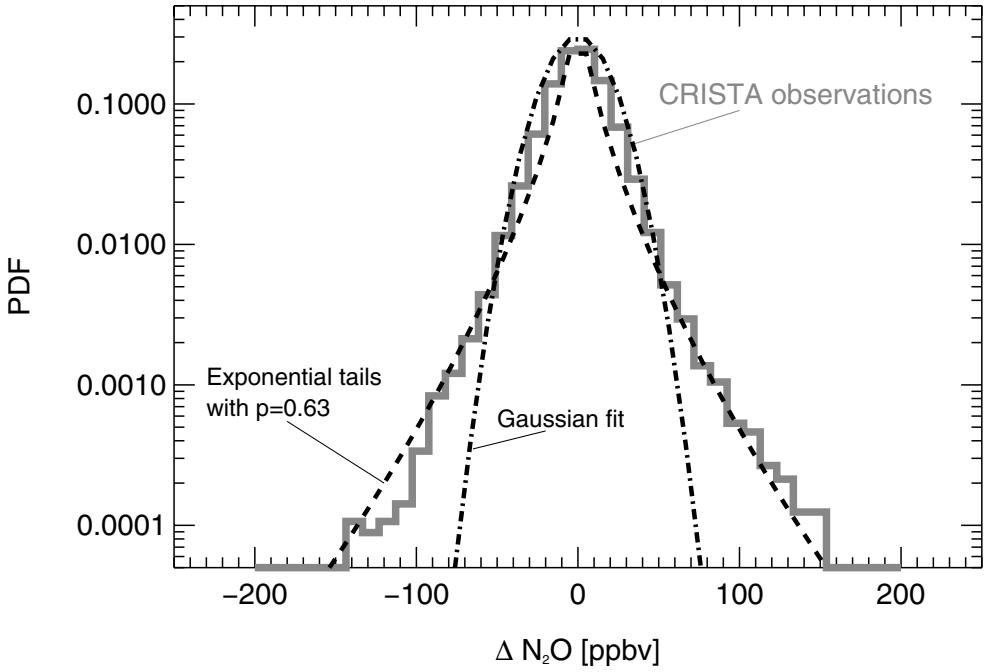

Figure 4. Probability density function (PDF) of N_2O differences derived from CRISTA data between 4 and 11 November (thick grey line). The dot-dashed line shows that the core of the observed PDF has a Gaussian shape. The tails of the PDF are fitted by an exponential function (dashed line). See text for details.

On the other hand, the shape of the simulated PDFs depends only weakly on the model resolution r_0. In Fig. 6, CLaMS PDFs for $r_0 = 45$, 65, 100 and 200 km are shown for pure advection studies ($\gamma_c = \infty$, Fig. 6(a)) and for $\gamma_c = 0.8$ (Fig. 6(b) to (d)). For these high-resolution simulations, computations would become numerically too expensive, so only a restricted domain was used between the south pole and 10°S. Consequentially, the PDFs calculated over this smaller domain have more pronounced non-Gaussian tails than Fig. 5, due to a stronger filamentation at the edge of the disturbed southern polar vortex.

6. Discussion

The CRISTA observations discussed in this paper provide a dataset with almost global coverage and with high spatial resolution resolving at least a part of the fine atmospheric structures manifested, for example, in the fat tails of the observed PDF of N_2O fluctuations (Fig. 4). The strong dependence of the shape of the simulated PDFs on the critical deformation γ_c justifies the use of this technique to quantify γ_c. An important advantage of using this technique is that observed and simulated tracer distributions can be compared even if the absolute positions of the simulated structures do not perfectly match the experimental data, e.g. due to inaccuracies in the meteorological wind fields or in the advection scheme. Such errors cannot significantly change the statistics of the tracer gradients and thus the shape of the PDFs.

Despite the comparatively high horizontal (200 km) and vertical (2–3 km) resolution, physical structures below these values are smoothed out by the CRISTA instrument (sometimes denoted as 'optical mixing' caused by the limited resolution of an optical

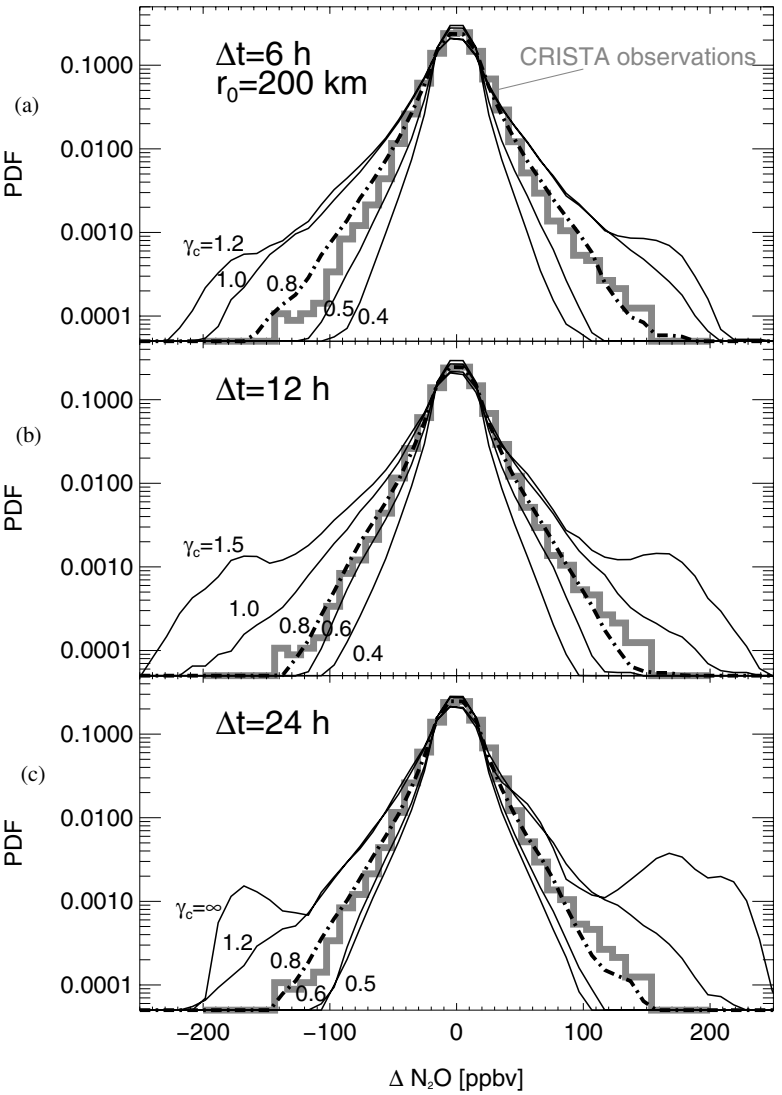

Figure 5. Probability density functions (PDFs) of N_2O differences derived from CRISTA data between 4 and 11 November (thick grey line) and corresponding CLaMS studies with $r_0 = 200$ km, Δt of (a) 6 hours, (b) 12 hours and (c) 24 hours, and different values of γ_c (thin lines). The best match (dot-dashed line) comes from $\gamma_c = 0.8$.

instrument). Therefore, even if the simulated tracer distributions (or PDFs) agreed with the observations, the underlying model diffusivity would only constitute an estimate of the upper bounds of the true atmospheric mixing intensity. Indeed, Sparling and Bacmeister (2001) have shown that the width of PDFs derived from *in situ* observations increases with the spatial resolution of the data. Thus, the critical horizontal deformation in CLaMS with $\gamma_c \approx 0.8$ derived from the comparison with the CRISTA data can only be understood as the lower bound of the real atmospheric deformations that trigger mixing.

Furthermore, our analysis shows a weak increase of the PDF width if the model resolution is increased as it is typical of fractal behaviour of the flow. Studying the PDFs of a tracer itself rather than PDFs of tracer differences, Hu and Pierrehumbert

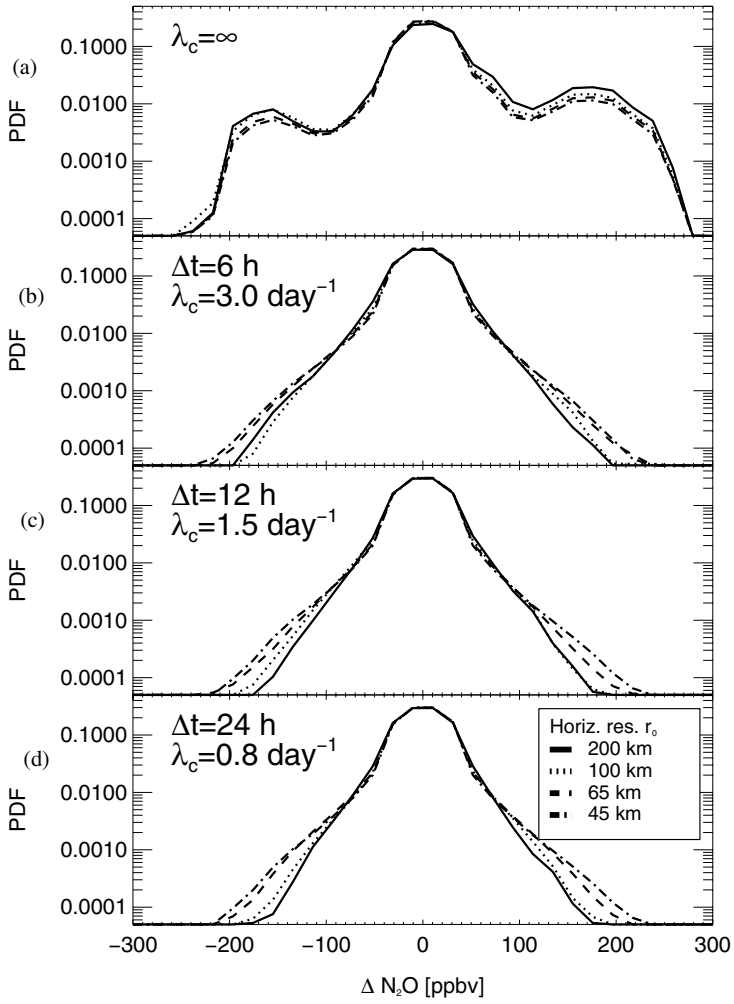

Figure 6. Scale dependence of the CLaMS PDFs derived from N_2O distributions southward of 10°S: (a) pure advection ($\lambda_c = \infty$) and (b), (c) and (d) with $\gamma_c = \lambda_c \Delta t = 0.8$, from different values of Δt and λ_c shown.

(2001) found a similar weak dependence of the simulated PDFs on the model resolution. We speculate that the resolution-dependent increase of the PDF width inferred from CLaMS simulations is too weak to compensate for the underestimate of γ_c due to a limited resolution of the CRISTA instrument.

The PDFs of tracers calculated with CLaMS for different periods and geographical regions (mainly in the middle and high latitudes) support the general results discussed in Sparling (2000). Using the optimized mixing parameters, the PDF width is smallest for the initial distribution and reaches a quasi-stationary state after about one week. The largest PDF width was derived from tracer distributions after the vortex break-up where strong filamentation dominates the spatial variability of the tracers.

Another way to illustrate the inhomogeneity of mixing is shown in Fig. 3(b) where CLaMS N_2O distribution is plotted for $\gamma_c = 0.8$ ($\Delta t = 12$ hours and $\lambda_c = 1.6$ s^{-1}). The white hatched contours indicate the areas with $\gamma > \gamma_c$, i.e. areas where (isentropic) mixing occurred during the last 12 hours. This area corresponds to only 12% of all APs

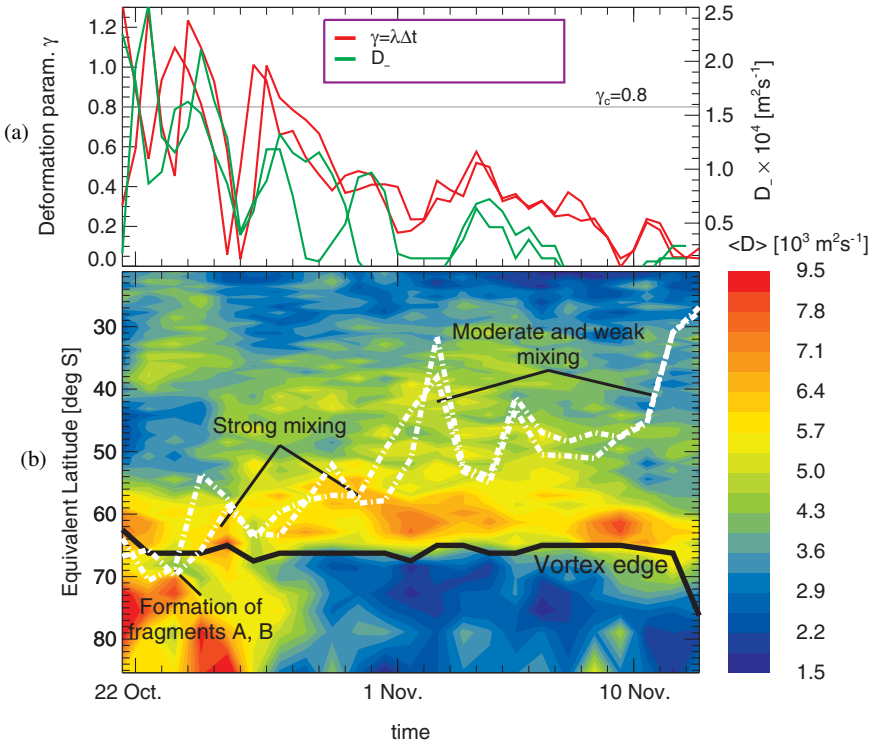

Figure 7. (a) History of the deformation parameter, γ, and the diffusion coefficient, D_-, along the trajectories following the vortex fragments A and B seen in Fig. 3. (b) Zonally averaged mixing intensity, $\langle D \rangle$, as a function of equivalent latitude in the vicinity of the vortex edge (thick black line). The white dashed lines are the trajectories of the vortex fragments A and B.

affected by the regridding procedure, with 15% as the highest value reached during the whole period considered.

The black line in Fig. 3(b) denotes the Antarctic vortex edge defined by the maximum gradient in PV (Nash *et al.* 1996). A strong inhomogeneity of mixing is evident that mainly occurs in the surf zone within the southern polar jet and along the streamers near the edge of the incipient northern vortex. The southern vortex edge separates the region of moderate mixing within the vortex and strong mixing in the outer flanks of the polar jet. The sharp gradients of N_2O at the vortex edge and two areas A and B of low N_2O mixing ratios between 20°S and 40°S are also evident both in the CLaMS distribution and in the corresponding CRISTA observations.

In Fig. 7 we show the mixing history that is responsible for the formation and transport of the vortex remnants A and B seen in Fig. 3(b). For this purpose, two representative trajectories starting on 20 October are considered. These trajectories connect the positions of the fragments every 12 hours during their transport from the vortex edge into midlatitudes. The deformation parameter γ (red) and the mean diffusion coefficient D_- (green) calculated along these trajectories are shown in Fig. 7(a). The parameter γ is calculated from the elongation of a circle with radius $r_0 = 50$ km surrounding each trajectory point. Using relation (1), D_- is calculated and averaged over all those nearest neighbours of the considered trajectory point which were created by merging of APs.

In Fig. 7(b), $\langle D \rangle$ denotes the zonally averaged value of D_- versus equivalent latitude (i.e. by using the latitude defined by transforming the area that is enclosed by a PV contour to a pole-centred circle of equal area), calculated for each day during the period considered. $\langle D \rangle$ estimates the meridional (or cross-vortex-edge) mixing intensity. Its greatest values occur outside the vortex edge (denoted by the black line) and between 21 and 24 October within the vortex. The white dashed curves are the equivalent latitudes of the trajectories following the mean positions of the fragments A and B. They start within the highly disturbed vortex and move equatorwards through regions of strong (until 30 October), moderate (between 31 October and 10 November) and weak (after 10 November) mixing.

A similar interpretation can be deduced from the deformation parameter γ and the diffusivity D_- calculated along the trajectories (Fig. 7(a)). Thus, until 28 October, the vortex remnants A and B were formed in the inner and outer flanks of the polar jet where conditions with $\gamma > 0.9$ were valid. In this phase of transport, the filaments were strongly elongated. After 1 November, the vortex fragments reached midlatitudes and experienced significantly smaller deformation rates with $\gamma < 0.5$. During this phase, the vortex fragments were mostly advected without significant mixing. The last CRISTA observations which show the existence of these fragments are on 11 November. In CLaMS simulation these fragments are clearly distinguishable until 15 November. Then both fragments are pushed back near the vortex edge where they quickly disappear owing to strong horizontal deformation rates in the outer flanks of the polar jet. Thus, we deduce their lifetime to be between 2 and 3 weeks.

Both the snapshot of the N_2O distribution in Fig. 3 and the zonally averaged mixing intensity $\langle D \rangle$ in Fig. 7 identify the vortex edge as a transport barrier preserving tracer gradients and separating regions with different mixing intensities. This kind of analysis complements the results which were obtained in terms of the effective diffusivity defined by Nakamura (1996). Haynes and Shuckburgh (2000) have shown that transport barriers such as the vortex edge or the subtropical jet are regions with small effective diffusivity. This is not surprising because the effective diffusivity measuring the stretching of tracer contours and the deformation-induced mixing as discussed here are strongly related concepts.

Finally, we would like to emphasize that the mixing algorithm in CLaMS works correctly only in a statistical sense, i.e. not every single mixing event caused by insertion or merging of APs necessarily has a physical realization. For example, the invariance of CLaMS PDF on the choice of Δt and λ_c by setting $\gamma_c = \lambda_c \Delta t = \text{constant}$ in the range $6 < \Delta t < 24$ hours means that even if the APs experience different 'mixing histories', their integral properties, i.e. their PDFs, are very similar. This means that frequently applied mixing with a high critical Lyapunov exponent λ_c produces similar PDFs compared with a rare use of the mixing algorithm with lower value of λ_c. Furthermore, as our first 3D studies show (Konopka *et al.* 2004), the value of the critical deformation γ_c increases up to values around 1.5 if, in addition to the horizontal strain, the vertical shear influences the deformation of the grid. Nevertheless, mixing in the 3D version of CLaMS remains strongly inhomogeneous and anisotropic.

7. Conclusions

The comparison of the isentropic CLaMS transport studies of N_2O with the CRISTA observations in terms of PDFs confirms the Lagrangian concept of strongly inhomogeneous and anisotropic mixing. The PDF of N_2O variability derived from CRISTA observations at 700 K shows non-Gaussian tails indicating strong filamentary

structures in the N_2O distributions, even if due to the resolution of the CRISTA instrument the strength of these tails may be underestimated. The critical deformation γ_c that triggers the mixing algorithm was estimated to be larger than 0.8, indicating that only a small part of the flow is affected by mixing. This means that mixing occurs very inhomogeneously, i.e. only in those parts of the flow where, on a time scale ≈12 hours and a spatial scale ≈200 km, a circle is deformed into an ellipse with the ratio between the major and minor axes exceeding 5. The anisotropy of mixing means that the diffusivity along the wind is greater than that across the wind by at least a factor of 25. Transport of vortex remnants into the midlatitudes, i.e. into regions with low deformation rates, may significantly increase their lifetime.

Acknowledgements

The UK Met Office is acknowledged for meteorological data support. We thank two anonymous reviewers for their constructive remarks.

References

Balluch, M. G. and Haynes, P. H. 1997 Quantification of lower stratospheric mixing processes using aircraft data. *J. Geophys. Res.*, **102,** 23487–23504

Dritschel, D. G. 1989 Contour dynamics and contour surgery: Numerical algorithm for extended, high-resolution modeling of vortex dynamics in two-dimensional, inviscid, incompressible flows. *Comput. Phys. Rep.*, **10,** 77–146

Edouard, S., Legras, B., Lefèvre, F. and Eymard, R. 1996 The effect of small-scale inhomogeneities on ozone depletion in the Arctic. *Nature*, **384,** 444–447

Haynes, P. and Anglade, J. 1997 The vertical scale cascade in atmospheric tracers due to large-scale differential advection. *J. Atmos. Sci.*, **54,** 1121–1136

Haynes, P. and Shuckburgh, E. 2000 Effective diffusivity as a diagnostic of atmospheric transport. 1: Stratosphere. *J. Geophys. Res.*, **105,** 22777–22794

Haynes, P. and Vanneste, J. 2004 Stratospheric tracer spectra. *J. Atmos. Sci.*, **61,** 161–178

Hu, Y. and Pierrehumbert, R. T. 2001 The advection-diffusion problem for stratospheric flow. Part I: Concentration probability distribution function. *J. Atmos. Sci.*, **57,** 1493–1510

Juckes, M. and McIntyre, M. 1987 A high-resolution, one-layer model of breaking planetary waves in the stratosphere. *Nature*, **328,** 590–596

Konopka, P., Grooß, J.-U., Bausch, S., Müller, R., McKenna, D. S., Morgenstern, O. and Orsolini, Y. 2003a Dynamics and chemistry of vortex remnants in late Arctic spring 1997 and 2000: Simulations with the Chemical Lagrangian Model of the Stratosphere (CLaMS). *Atmos. Chem. Phys.*, **3,** 839–849

Konopka,P., Grooß, J.-U., Günther, G., McKenna, D. S., Müller, R., Elkins, J. W., Fahey, D. and Popp, P. 2003b Weak impact of mixing on chlorine deactivation during SOLVE/THESEO2000: Lagrangian modeling (CLaMS) versus ER-2 in situ observations. *J. Geophys. Res.*, **108,** 8324, doi:10.1029/2001JD000876

Konopka, P., Steinhorst, H.-M., Grooß, J.-U., Günther, G., Müller, R., Elkins, J. W., Jost, H.-J., Richard, E., Schmidt, U., Toon, G. and McKenna, D. S. 2004 Mixing and ozone loss in the 1999-2000 arctic vortex: Simulations with the 3-dimensional Chemical Lagrangian Model of the Stratosphere (CLaMS). *J. Geophys. Res.*, **109,** doi:10.1029/2003JD003792

Kouker, W., Offermann, D., Küll, V., Reddmann, T., Ruhnke, R. and Franzen, A. 1999 Streamers observed by the CRISTA experiment and simulated in the KASIMA model. *J. Geophys. Res.*, **104,** 16405–16418

McIntyre, M. E. and Palmer, T. N. 1983 Breaking planetary waves in the stratosphere, *Nature*, **305,** 593–600

McKenna, D. S., Konopka, P., Grooß, J.-U., Günther, G., Müller, R., Spang, R., Offermann, D. and Orsolini, Y. 2002 A new Chemical Lagrangian Model of the Stratosphere (CLaMS). Part I: Formulation of advection and mixing. *J. Geophys. Res.*, **107,** 4309, doi:10.1029/2000JD000114

Nakamura, N. 1996 Two-dimensional mixing, edge formation, and permeability diagnosed in area coordinates. *J. Atmos. Sci.*, **53,** 1524–1537

Nash, E. R., Newman, P. A., Rosenfield, J. E. and Schoeberl, M. R. 1996 An objective determination of the polar vortex using Ertel's potential vorticity. *J. Geophys. Res.*, **101,** 9471–9478

Ngan, K. and Shepherd, T. G. 1999a A closer look at chaotic advection in the stratosphere. Part I: Geometric structure. *J. Atmos. Sci.*, **56,** 4134–4152

1999b A closer look at chaotic advection in the stratosphere. Part II: Statistical diagnostics. *J. Atmos. Sci.*, **56,** 4153–4166

Norton, W. A. 1994 Breaking Rossby waves in a model stratosphere diagnosed by a vortex-following coordinate system and a technique for advecting material contours. *J. Atmos. Sci.*, **51,** 654–673

Offermann, D., Grossmann, K.-U., Barthol, P., Knieling, P., Riese, M. and Trant, R. 1999 Cryogenic Infrared Spectrometers and Telescopes for the Atmosphere (CRISTA) experiment and middle atmosphere variability. *J. Geophys. Res.*, **104,** 16311–16325

Orsolini, Y. J., Hansen, G., Hoppe, U. P., Manney, G. L. and Fricke, K. H. 1997 Dynamical modelling of wintertime lidar observations in the Arctic. *Q. J. R. Meteorol. Soc.*, **123,** 785–800

Pierrehumbert, R. T. 1991 Large-scale horizontal mixing in planetary atmospheres. *Phys. Atmos. Fluids*, **3A,** 1250–1260

Prather, M. J. 1986 Numerical advection by conservation of second-order moments. *J. Geophys. Res.*, **91,** 6671–6681

Riese, M., Tie, X., Brasseur, G. and Offermann, D. 1999 Three-dimensional simulation of stratospheric trace gas distributions measured by CRISTA. *J. Geophys. Res.*, **104,** 16419–16435

Searle, K. R., Chipperfield, M. P., Bekki, S. and Pyle, J. A. 1998 The impact of spatial averaging on calculated polar ozone loss: I. Model experiments. *J. Geophys. Res.*, **103,** 25397–25408

Shraiman, B. and Siggia, E. D. 2000 Scalar turbulence. *Nature*, **405,** 639–646

Sparling, L. C. 2000 Statistical perspectives on stratospheric transport. *Rev. Geophys.*, **38,** 417–436

Sparling, L. C. and Bacmeister, J. T. 2001 Scale dependence of tracer microstructure: PDFs, intermittency and the dissipation scale. *J. Geophys. Res.*, **28**, 2823–2826

Sutton, R. T., Maclean, H., Swinbank, R., O'Neill, A. and Taylor, F. W. 1994 High-resolution stratospheric tracer fields estimated from satellite observations using Lagrangian trajectory calculations. *J. Atmos. Sci.*, **51,** 2995–3005

Tan, D. G. H., Haynes, P. H., MacKenzie, A. R. and Pyle, J. A. 1998 Effects of fluid-dynamical stirring and mixing on the deactivation of stratospheric chlorine. *J. Geophys. Res.*, **103,** 1585–1605

Tuck, A. F., Hovde, S. J., Gao, R. S. and Richard, E. C. 2003 Law of mass action in the Arctic lower stratospheric polar vortex January-March 2000: ClO scaling and the calculation of ozone loss rates in a turbulent fractal medium. *J. Geophys. Res.*, **108,** 4451, doi:10.1029/2002JD002832

Waugh, D. W. and Plumb, R. A. 1994 Contour advection with surgery: A technique for investigating finescale structure in tracer transport. *J. Atmos. Sci.*, **51,** 530–540

Waugh, D. W., Plumb, R. A., Elkins, J. W., Fahey, D. W., Boering, K. A., Dutton, G. S., Volk, C. M., Keim, E., Gao, R.-S., Daube, B. C., Wofsy, S. C., Loewenstein, M., Podolske, J. R., Chan, K. R., Proffitt, M. H., Kelly, K. K., Newman, P. A. and Lait, L. R. 1997 Mixing of polar vortex air into middle latitudes as revealed by tracer-tracer scatterplots. *J. Geophys. Res.*, **102,** 13119–13134